

Proceedings of the 26th Polish Seminar on Positron Annihilation, Pokrzywna 1994

# “RIDGE” FERMI SURFACE STUDY IN METALLIC (R)Ba<sub>2</sub>Cu<sub>3</sub>O<sub>7- $\delta$</sub> (R = Y, Dy) AND IN OXYGEN DEFICIENT YBa<sub>2</sub>Cu<sub>3</sub>O<sub>7- $\delta$</sub> BY POSITRON ANNIHILATION

L. HOFFMANN, A.A. MANUEL, B. BARBIELLINI\*, M. PETER, A. SHUKLA  
AND E. WALKER

Département de Physique de la Matière Condensée, Université de Genève  
24 Quai E. Ansermet, 1211 Genève 4, Switzerland

We present a detailed positron 2D-ACAR measurements study of the “ridge” Fermi surface of (R)Ba<sub>2</sub>Cu<sub>3</sub>O<sub>7- $\delta$</sub>  (R = Y, Dy) compared to full-potential linearized augmented plane wave and linear muffin-tin orbital calculations. From different 2D-ACAR projections measured in DyBa<sub>2</sub>Cu<sub>3</sub>O<sub>7- $\delta$</sub> , a 3D model of the momentum density of the ridge was established and is in good agreement with LMTO calculations of YBa<sub>2</sub>Cu<sub>3</sub>O<sub>7</sub>, confirming the description of the ridge Fermi surface by local density approximation calculations. The ridge is also studied in oxygen deficient YBa<sub>2</sub>Cu<sub>3</sub>O<sub>7- $\delta$</sub> . With growing  $\delta$ , the ridge disappears without changing in width. This is consistent with full-potential linearized augmented plane wave calculations of YBa<sub>2</sub>Cu<sub>3</sub>O<sub>6.5</sub>, and supports the phase separation model of Mesot et al.

PACS numbers: 71.25.Hc, 74.72.Bk, 74.72.Jt, 78.70.Bj

## 1. Introduction

Fermi surfaces (FS) of the high critical temperature ( $T_c$ ) superconductors have been largely studied [1] using two-dimensional angular correlation of annihilation radiation (2D-ACAR) [2]. In YBa<sub>2</sub>Cu<sub>3</sub>O<sub>7</sub>, full-potential linearized augmented plane wave (FLAPW) band structure calculations [3] predict four FS sheets: two FS centered around the  $S$  point (Brillouin zone (BZ) corner) made of holes in shape of “barrels” find their origin in the CuO<sub>2</sub> plane states, a one-dimensional electron plane-like “ridge” FS along  $\Gamma X$  due to the CuO chain states, and finally a hole FS in shape of a “pillbox”, located at the  $S$  point with contributions from both the CuO chain and the CuO<sub>2</sub> plane. The positron wave function is mainly localized in the interstitial space along the CuO chains [4–7]. Therefore only the FS features related to the CuO chain states, i.e. the ridge FS and the pillbox FS,

\*Present address: Laboratory of Physics, Helsinki University of Technology, 02150 Espoo, Finland.

are expected to be observed by 2D-ACAR. After having found some indications of the pillbox FS signal [8, 9], the pillbox FS was clearly made evident recently [10]. The ridge FS has been clearly identified by 2D-ACAR measurements in untwinned samples [8, 11, 12] and even in twinned samples [13]. Further characterization of the ridge FS by substituting a few percent of the Cu atoms by other metallic atoms  $M$  [14] shows that for  $M = \text{Ni}, \text{Zn}$  the ridge FS remains unchanged, whereas for  $M = \text{Al}$  the ridge FS is destroyed since the Al atoms replace the Cu atoms of the chains. No relation between  $T_c$  of the substituted compounds and the ridge signal could be established leading to the conclusion that the CuO chains are not essential for superconductivity. From 2D-ACAR measurements in  $(\text{R})\text{Ba}_2\text{Cu}_3\text{O}_{7-\delta}$  where the rare earth  $\text{R} = \text{Dy}, \text{Ho}$  and  $\text{Pr}$  [15], it was found that the ridge signal is not affected by the substitution of Y by the rare earth elements, even in the semi-conducting  $\text{PrBa}_2\text{Cu}_3\text{O}_{7-\delta}$  compound, where the macroscopic insulating behavior is ascribed to disorder in CuO chains which however remain metallic at microscopic level.

In this paper, we discuss in detail the ridge FS signal in the 2D-ACAR spectra of  $\text{YBa}_2\text{Cu}_3\text{O}_{7-\delta}$ , as seen by the experiment, and as predicted by FLAPW and linear muffin-tin orbital (LMTO) calculations. The novelty is the angular projections of the ridge FS measured in  $\text{DyBa}_2\text{Cu}_3\text{O}_{7-\delta}$  in the  $ac$  plane and in the  $bc$  plane, from which we deduce a 3D model of the momentum density of the ridge FS, and compare it with LMTO calculations of  $\text{YBa}_2\text{Cu}_3\text{O}_7$ . We also present another original study of the evolution of the ridge FS in  $\text{YBa}_2\text{Cu}_3\text{O}_{7-\delta}$  as a function of oxygen deficiency  $\delta$ , compared to other experiments and to FLAPW calculations.

The ridge FS induced structures are weak and the statistical noise of the 2D-ACAR histogram becomes competitive in intensity. We assume that the shape and position of the ridge FS signal are known, whereas we are interested in measuring its width and intensity. Let the vector  $D$  be a section through the measured 2D-ACAR.  $D$  can be expressed matricially as  $D = K\Phi + N$ , where  $K$  is a matrix containing centered square functions of equal intensity but of different width, the vector  $\Phi$  selects and weights the square functions of  $K$  which are present in the data  $D$ , and  $N$  is the additional statistical noise. The problem is to extract  $\Phi$  knowing  $K$  and  $D$ . This is an inverse problem. We have developed a filtering technique [16] solving the problem optimally. First a filter  $F$  is calculated. Its expression is  $F = (C_\Phi K^T)/(KC_\Phi K^T + C_N)$ , where  $C_\Phi$  is the autocorrelation matrix of  $\Phi$  and  $C_N$  that of the noise. Then, the regularized solution  $\Phi_R$  is obtained by applying this filter on the section  $D$ :  $\Phi_R = FD$ . In the following ridge FS study, we take a set of sections perpendicular to the ridge from the  $\Gamma$  point up to  $p_a = 8.1$  mrad, all 1.35 mrad wide. Each section is filtered individually by the same filter, applied twice to sharpen the structures. The set of parameters chosen for the filter (signal to noise ratio of 3, a Gaussian resolution of  $\sigma = 0.3$  mrad) is the same for all sections, and is therefore not optimal for each section simultaneously. This slightly influences the filtered result, but the features discussed below have the same trends independently of the choice of the set of parameters. In order to have a comparable scale for the filtered data, all the 2D-ACAR shown below were normalized to the same volume ( $10^8$ ) before filtering.

## 2. Ridge FS signal in the 2D-ACAR spectra for $\text{YBa}_2\text{Cu}_3\text{O}_{7-\delta}$

Let us first have an idea of the intensity of the measured ridge FS signal. From a high statistics ( $10^9$  counts) 2D-ACAR measurement performed at  $T = 300$  K and integrated along the  $c$ -axis [15] in a high quality ( $T_c = 93.1 \pm 1$  K) untwinned  $\text{YBa}_2\text{Cu}_3\text{O}_{7-\delta}$  single crystal, the magnitude of the ridge FS signal is estimated as 0.8% of the 2D-ACAR maximum in the 1st BZ. In the 2nd and 3rd BZ, the 1st and 2nd Umklapp components of the ridge FS signals lie around 0.4% and 0.1%, respectively. For  $10^8$  counts, the statistical error per  $\text{mrad}^2$  normalized to the 2D-ACAR maximum is about 0.13% in the center of the distribution, 0.09% and 0.03% in 2nd and 3rd BZ, respectively. Therefore, for  $1 \text{ mrad}^2$  resolution, the ridge FS may be observed in the three BZ, however for a detailed study such a resolution is too low since it is of the order of magnitude of the ridge FS width itself. In higher resolution data, one can enhance the ridge FS signal with respect to the noise, by superposing all Umklapp components of the ridge together, summing the data translated by  $p_b = 0, \pm 2\pi/b$  and  $\pm 4\pi/b$ . For larger  $p_b$  values the ridge FS signal contribution becomes very small and is neglected. This folding procedure doubles the intensity of the ridge FS signal whereas the noise is only enhanced by a factor  $\sqrt{2}$ , and moreover, it has the additional advantage of partially eliminating other modulations induced by wave function effects which do not have the reciprocal lattice periodicity. These are low frequency modulations and are again reduced by high pass Fourier filtering. Recently a similar Fourier filtering was applied successfully by the Arlington group [17] to enhance the FS features. Now the ridge FS lies centered on a well defined straight line along  $p_a$  ( $p_c = \text{integration direction, } p_b = 0$ ). We applied the above described filter  $F$  on the 2D-ACAR. The result is shown in Fig. 1a. Since, in the 2D-ACAR, we are interested in ridge-like features, only positive amplitudes are shown in Fig. 1. The negative ones, signatures of valley-like trends, have been truncated. One coordinate of the basal plane is the momentum in the  $a$  direction, and the other represents the half width (in  $\text{mrad}$ ) of the ridge-like structures. The heights of filtered structures are related to the amplitudes of the ridge-like breaks present in the 2D-ACAR. More precisely, the volumes of the filtered structures (after integration along the half ridge width coordinate) have to be considered, since they remain constant whatever the choice of the filter parameters is, in contrast with the shape of the filtered structure, which becomes higher and narrower for large signal to noise ratio or for more sharp edged ridges. This is not surprising since the filtered data may be considered as a kind of derivative of the 2D-ACAR along the half ridge width coordinate. The ridge FS signal intensities discussed in this paper were estimated in this way. In Fig. 1a, one observes an elongated structure at  $0.6 \pm 0.1 \text{ mrad}$  half width labelled  $R$ , extended up to  $p_a \approx 6 \text{ mrad}$  and with variable height. It is the signature of the ridge FS. An additional wider structure around  $p_a \approx 4 \text{ mrad}$ , labelled  $W$ , is made evident and interpreted as an effect of the wave functions.

The filtered (and folded) FLAPW band structure calculations [6] of  $\text{YBa}_2\text{Cu}_3\text{O}_7$  is shown in Fig. 1b. The smoothing, corresponding to the experimental momentum resolution, has no significant effect in the filtered result, and is neglected. As in the experiment (Fig. 1a), FLAPW predicts an elongated struc-

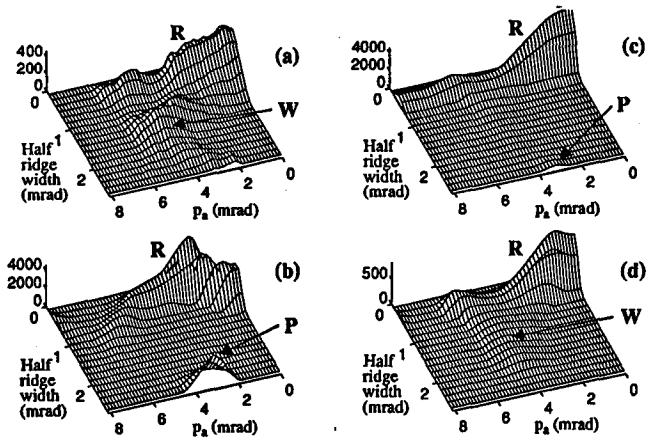


Fig. 1. Filtered normalized 2D-ACAR of  $\text{YBa}_2\text{Cu}_3\text{O}_{7-\delta}$  integrated along the  $c$ -axis. Coordinates of the basal plane:  $p_a$ , and the half width of the ridge-like structures. Vertical scale: arbitrary. Only the positive amplitudes are shown. (a) Experiment, (b) FLAPW calculations, (c) LMTO calculations, (d) LMTO calculations with FS signal reduced to 30%.  $R$  is for ridge,  $W$  for wave function and  $P$  for pillbox.

ture  $R$ , the ridge FS. The ratio between the volume (after integration along the half ridge width coordinate) of the calculated and measured  $R$  is close to 5. In the experiment (Fig. 1a), the maximum of  $R$  is one order of magnitude smaller than predicted by FLAPW (Fig. 1b), which means that we measure not a unique ridge but a broadened distribution of ridges. We observed that this broadening is induced by the folding procedure, due to an additional weak and wider ridge-like component, appearing in the 2nd and 3rd BZ. This is consistent with the broad distribution observed in our LCW(Lock, Crisp, West)-folded data [18] (where all BZ are folded back in the 1st BZ), instead of sharp discontinuities. The origin of this broadening is very likely due to perturbations caused by wave functions. Therefore, the volume of  $R$  should be more enhanced by the folding procedure for the experiment (due to the additional wave functions) than for FLAPW. But this is not the case, the ratio 5 between the measured and calculated  $R$  volumes remains, and we may conclude that FLAPW overestimates the signals of the 1st and 2nd Umklapp components of the ridge FS by a factor larger than 5. This is confirmed by filtering out the ridge FS individually in the 2nd and 3rd BZ (not shown). Now, if we examine more in detail the calculated  $R$  (Fig. 1b), we observe an increase in width at the  $\Gamma$  points ( $p_a = 0$  and  $6.3$  mrad) due to the dispersion of the ridge width in the  $ac$  plane. This modulation in width is not observed in the experiment at  $T = 300$  K. However recent measurements at  $T = 450$  K reproduce the same modulation as given by FLAPW, suggesting sensitivity of the measured ridge FS dispersion to positron traps. But small width modulations may also be induced by noise, therefore we do not interpret them in this paper (except the large increase in width observed in the data with the integration direction tilted in the  $b$  direction). The measuring temperature does not influence the intensity of

$R$ , on which we base our interpretations of the ridge FS momentum density shown later. In Fig. 1b, the filter completely suppresses the effect of wave functions  $W$  observed experimentally, due to the dominant FS signal. At  $p_a = 3.15$  mrad a pointed structure appears nearly 3 mrad in half width, labelled  $P$ , which is the signature of the pillbox FS. This piece of FS is not detected in this measurement (Fig. 1a). We interpret this as an effect of positron trapping, confirmed by recent measurements at  $T = 400$  K which clearly reveal the pillbox FS [10].

The 2D-ACAR calculated using the LMTO formalism reproduces the main trends of FLAPW, but is distinguished by small differences. In the filtered (volume normalized) 2D-ACAR shown in Fig. 1c, the dominating structure is the ridge FS  $R$ . Its half width of 0.8 mrad is constant and much smaller than that of FLAPW. This is due to the limited resolution used in LMTO which is  $\approx 0.8$  mrad in the  $ab$  plane. Therefore, a finer mesh is needed to study more in detail the ridge width dispersion from LMTO. However the intensity is less affected by the resolution. Compared to FLAPW,  $R$  is 30% more intense, a precise value can not be estimated since some slightly different modulations are also observed. The pillbox FS from LMTO, the small bump  $P$  of nearly 3 mrad half width at  $p_a = 3.15$  mrad, is much weaker than in FLAPW, partially due to the coarse mesh used (only one point is concerned). On comparing FLAPW and LMTO with experiments, it seems that both methods give similar features, but as far as quantitative details are concerned, FLAPW is closer to the measured data. But neither method gives a perfect description of the electronic structure for  $\text{YBa}_2\text{Cu}_3\text{O}_7$  as we shall see later. Both use the local density approximation (LDA), but a rigorous calculation should go beyond LDA. For example it has been shown [19] that  $d$ -electrons are less sampled by positrons than predicted by LDA calculations including electron-positron correlations, and this may be explained by electron-electron correlations which are neglected.

The fact that the calculated signals in the momentum distribution are much stronger than the measured ones is still not understood. In general the structures seen in the experiment agree with the theory, but are present in a smaller fraction. We have dealt with this question earlier [18] and we come back to it again in this paper. One possible answer could be that the positrons sample only partially the material, due to positron trapping mechanisms in vacancies. We studied the positron trapping using lifetime measurements [10], and the conclusion is that in  $\text{YBa}_2\text{Cu}_3\text{O}_{7-\delta}$ , traps exist and are localized in chain oxygen vacancies. These are shallow traps, and at  $T > 400$  K their effect is negligible. 2D-ACAR measurements, performed at  $T = 300$  K and  $T = 400$  K, do not show a significant temperature effect on the 2D-ACAR anisotropy. The experimental magnitude is roughly one third of the theoretical one, and no significant enhancement of the ridge FS signal is observed. This does not explain the difference of five between the experiment and the theory. On the other side, in the calculations, a lot of care was taken in the description of the positron-electron correlations by mean of an enhancement factor [20], which largely influences the calculated annihilation rate. The agreement of the positron lifetime value for  $\text{YBa}_2\text{Cu}_3\text{O}_7$  between the calculations (157–165 ps) and the experiment ( $165 \pm 2$  ps) is satisfactory [21], which means that the introduction of correlation effects in the calculations improves a

lot the agreement with the experiment. Such correlation effects act on the FS signal intensity, and were already taken into account in the calculations presented here. What is not taken into account is the electron–electron interaction, which reduces and eventually smears out the FS breaks. On this subject, there exists a new idea [22] which stipulates that this effect is very large except in a range of 20 meV around the Fermi energy ( $E_F$ ). For states very close to  $E_F$ , the screening is ionic (instead of electronic) and has no smearing effect. In the momentum distribution, ionic screening makes the FS breaks appearing locally around  $p_F$ , whereas beyond  $p_F$ , the distribution reflects the smeared out break. The local FS induced breaks should come out clearly in high resolution data. However for the finite experimental momentum resolution we have, limited by the detectors and the measuring temperature (thermal broadening), the FS induced signal is simply reduced. Further high resolution measurements are worth undertaking to clearly identify this effect.

For a better comparison between experiment and theory, we may normalize to the amplitude of the anisotropy of the 2D-ACAR, instead of to the total volume. The anisotropy is obtained after having subtracted from the 2D-ACAR its cylindrical average. The magnitude of the anisotropic part in the LMTO case is twice as large as in the experiment. After this normalization we expect that the wave functions have similar magnitudes in both experiment and LMTO, since the anisotropy is dominated by wave functions. But even in this scale, the LMTO FS signal exceeds the measured one roughly by a factor of 3. With this in mind we reduced in LMTO the FS signal to 30% of its initial intensity, by replacing 70% of the calculated 2D-ACAR volume by a calculation, where the Fermi level was shifted above the partially filled bands giving a 2D-ACAR without FS breaks (both calculations were performed for the  $O_7$  compound). The filtered result for the modified LMTO calculations is shown in Fig. 1d. One observes, compared to Fig. 1c, the expected reduction of 30% of  $R$ , and also enhancement of the wave functions  $W$  at  $p_a \approx 4$  mrad, which becomes comparable to the experiment (Fig. 1a), despite the separation between  $R$  and  $W$  resolved in the experiment but not in LMTO. The maximum of  $R$  is higher than in the experiment, but the total signals (volume of  $R$ ) are similar, due to the more broader character of the ridge FS in the experiment, induced by the folding as discussed above.  $R$  disappears at  $p_a$  larger than 6 mrad as in the experiment, and also the neck at  $p_a \approx 4$  mrad is more pronounced in the modified calculation and agrees better with the experiment. For reasons of convenience as regards calculations, we chose the LMTO method to calculate all the different 2D-ACAR projections used below for the comparison with the experiment, and they have all been modified to reduce the FS signal as described above, for better comparison.

### 3. Ridge FS momentum density in $DyBa_2Cu_3O_{7-\delta}$

We have observed that the substitution of the Y atoms in  $YBa_2Cu_3O_{7-\delta}$  by various rare earths does not affect the 2D-ACAR spectra, and concluded that their electronic structures are very similar [15]. The present study of the ridge FS has been made on a high quality untwinned  $DyBa_2Cu_3O_{7-\delta}$  single crystal. The

$2 \times 1 \times 0.1 \text{ mm}^3$  sample was grown from  $\text{Dy}_2\text{O}_3$ ,  $\text{BaO}$  and  $\text{CuO}$  powders using a flux technique [23]. The sample was soaked at  $1030^\circ\text{C}$ , slow-cooled ( $0.8^\circ\text{C}/\text{hour}$ ) from  $985^\circ\text{C}$  down to  $940^\circ\text{C}$ , and further oxidized for 5 hours at  $600^\circ\text{C}$  and 12 days at  $400^\circ\text{C}$ . The superconducting transition temperature  $T_c = 85.5 \text{ K}$  was determined by AC susceptibility ( $\chi_{AC}$ ) measurements. The sample was untwinned using the technique described in Ref. [24]. Under polarized light, it was observed that more than 95% of the sample was twin-free. Seven 2D-ACAR spectra were measured at  $T = 300 \text{ K}$  for different crystal orientations, varying the direction of integration in the plane of the ridge between the  $c$  and  $a$  axes by steps of  $22.5$  degrees. In the  $bc$  plane, 2 measurements at  $10$  and  $20$  degrees from the  $c$ -axis were performed. The statistics vary between  $1.13 \times 10^8$  and  $3.61 \times 10^8$  counts.

In the following study, we mainly focus our interest on the contribution of the ridge FS in the momentum density space  $p$  (the extended zone representation). It should be noted that, in  $p$  space, the extension of a FS may cover several BZ, depending upon the localization in real space of the electron and positron states. However the dispersion in width of a plane-like FS in  $p$  space (its deviation from a plane) depends only on that in the reduced  $k$  space (in the first BZ). Therefore the dispersion pattern of the plane-like FS in  $p$  space is periodically repeated in each BZ.

Figure 2 shows the filtered 2D-ACAR measured in  $\text{DyBa}_2\text{Cu}_3\text{O}_{7-\delta}$  in the  $ac$  plane (left column), and the corresponding calculations performed for  $\text{YBa}_2\text{Cu}_3\text{O}_7$  using the LMTO method (right column). The main trends deduced are the following. From  $c$  projection (Fig. 2a) to  $a$  projection (Fig. 2e), the ridge extension  $R$  increases for both experiment and calculations, whereas its maximum globally decreases, suggesting that the momentum density of the ridge is longer in the  $c$  direction than in the  $a$  direction. From a more detailed analysis, we conclude that in the  $ac$  plane the ridge momentum density is concentrated in a centered rectangle of about  $5 \times 15 \text{ mrad}^2$ . A comparison between the two measured projections  $a$  and  $c$  was performed earlier by Smedskjaer et al. [25] concluding that the ridge FS is an approximately flat surface but they drew no conclusions about its non-planarity. In the experiment (left column), we observe some modulations of the ridge FS width. These modulations are either in regions, where the ridge signal is weak and sensitive to perturbations, or they are due to the presence of second wider components  $W$ . All the  $W$  components, however less marked and not always resolved from  $R$ , are also present in the calculations (right column), and reflect some residual wave function effects. The  $c$  projection seems the least affected by these perturbations and does not show significant dispersion in the ridge width. The same conclusion is drawn from the high statistics data (Fig. 1a) of  $\text{YBa}_2\text{Cu}_3\text{O}_{7-\delta}$ , where the average ridge FS width is estimated to about  $0.6 \pm 0.1 \text{ mrad}$  half width. If we look at Fig. 2a more in detail, we observe that, both in the calculations and in the experiment, the intensity modulation along the ridge suggests a strong centered momentum density component ( $R$ ) and weaker subsidiary structures around  $p_a = 5 \text{ mrad}$  (labelled  $s$ ). The more hilly nature of the experiment is a signature of the statistical noise, and reveal the weakness of the FS signal in the measured data as discussed above. In Figs. 2b to 2d, we observe in the experiment the wave function component  $W$  appearing at  $\Gamma$  point ( $0 \text{ mrad}$ ) in (b), clearly visible in (c)

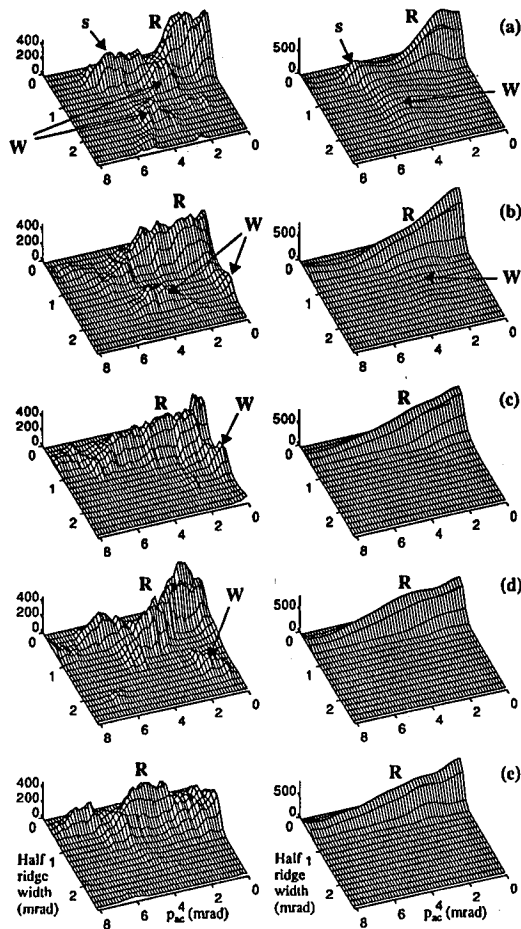


Fig. 2. Filtered normalized 2D-ACAR. The integration direction is in the  $ac$  plane. Coordinates of the basal plane: momentum in the  $ac$  plane perpendicular to the integration direction, and the half width of the ridge-like structures. Vertical scale: arbitrary. Only the positive amplitudes are shown. Measurements of  $\text{DyBa}_2\text{Cu}_3\text{O}_{7-\delta}$  (left column) and LMTO calculations of  $\text{YBa}_2\text{Cu}_3\text{O}_7$  (right column) integrated between  $c$ -axis (a) and  $a$ -axis (e) spaced by 22.5 degrees.  $R$  is for ridge,  $W$  for wave function and  $s$  for subsidiary structure.

and shifted to the left in (d). In the calculations this effect is present but much less pronounced. The intensity of the  $W$  components is very sensitive to the shape and to the angle at which the wave functions are projected, influencing their dominance in the filtered spectra. Therefore, the same 3D structure has different dominant features for differently oriented projections. For this reason, the  $W$  component clearly seen at  $p_a \approx 4$  mrad in Figs. 2a and 2b disappears in (c), (d) and (e).

In Fig. 3, the integration directions are in the  $bc$  plane, 10 degrees (a) and 20 degrees (b) from the  $c$ -axis. Tilted by 10 degrees (Fig. 3a), the experiment (left



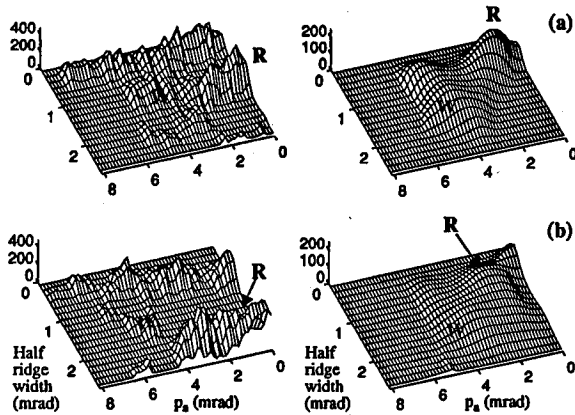


Fig. 3. Filtered normalized 2D-ACAR of  $\text{YBa}_2\text{Cu}_3\text{O}_{7-\delta}$ . The integration direction is in the  $bc$  plane. Coordinates of the basal plane:  $p_a$ , and the half width of the ridge-like structures. Vertical scale: arbitrary. Only the positive amplitudes are shown. The integration direction is at 10 degrees (a) and 20 degrees (b) from the  $c$ -axis. Left column: experiment, right column: LMTO calculations.  $R$  is for ridge,  $W$  for wave function.

column) shows a weakening of the signal from the ridge  $R$ , and a widening up to 1.3 mrad half width. Such a width is achieved by a ridge of about 15 mrad in length along the  $c$  direction, compatible with the ridge length along  $p_c$  in Fig. 2e. Further tilting (Fig. 3b) still increases the ridge width in agreement with the previous estimation. We also observe the presence of another ridge-like structure, narrower than the ridge FS ( $\approx 0.3$  mrad) for the integration tilted 10 degree from  $c$  (and wider for the 20 degree case). This feature does not directly reflect the ridge FS momentum density extension (since it is narrower than its width), and is therefore not interpreted. Its origin is probably similar to that associated to the wave functions  $W$  seen in Fig. 2. In the calculations (Fig. 3, right column), the ridge width also increases with respect to the angle, but in a smaller proportion than in the experiment. The origin of this difference is partially due to the limited resolution used in LMTO leading to a narrow ridge FS (only one plane is concerned), and may also be due to the different ways in which the ridge momentum density decreases along the  $c$ -axis, indeed the measured structures (Fig. 3 left) are more pronounced than the calculated ones (Fig. 3 right) as seen in Fig. 2.

In Fig. 4, we show the comparison between theory and the model derived from the measurements, of the ridge momentum density. The gray scale image with contour lines is the picture from LMTO. The superimposed thick full lines represent our schematic model and delimit the region where the momentum density is concentrated. One observes the overall good agreement. In both cases, the size of the central contribution is comparable, and the subsidiary structures around  $p_a = \pm 5$  mrad are present. One clearly sees the decrease in the ridge momentum density along the  $c$ -axis, which may be slightly different in the experiment giving rise to the different ridge width increase as shown in Fig. 3. The physical origin of the ridge momentum density extension along the  $c$ -axis reflects the localization

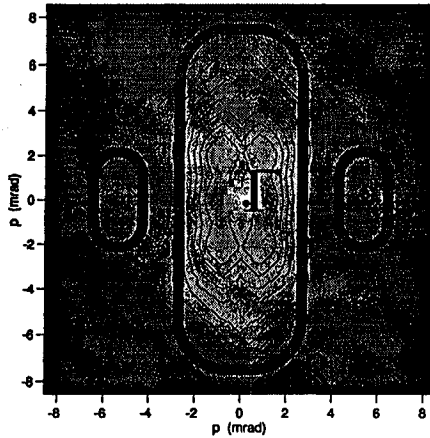


Fig. 4. 3D momentum density of the ridge in the  $ac$  plane. Thick full lines: model sketched from the measurements in  $\text{DyBa}_2\text{Cu}_3\text{O}_{7-\delta}$ . These lines delimit the region of high momentum density.  $R$  is for the ridge and  $s$  for the subsidiary structure. Thin contour lines and gray scale: LMTO calculations in  $\text{YBa}_2\text{Cu}_3\text{O}_7$ . Dark is low.

of the electrons in the  $ab$  plane. This is not surprising since the electronic states sampled by the positrons belong mainly to the  $\text{CuO}$  chains lying along the  $b$  direction. It is difficult to interpret the structures more in detail, since the features in the filtered data are weak and comparable to noise induced modulations. We should remember that the following reasons may also partially account for disagreements between experiment and theory: the precision of the calculations, the limited sample quality, the limited statistics, the partially trapped positrons due to the measuring temperature ( $T = 300$  K), and the different rare earth in the experiment (Dy) and in the calculations (Y) which show similar 2D-ACAR spectra [15] but may be different as concerns details. We may therefore consider the overall agreement as satisfactory.

#### 4. 2D-ACAR in oxygen deficient $\text{YBa}_2\text{Cu}_3\text{O}_{7-\delta}$

The  $\text{YBa}_2\text{Cu}_3\text{O}_{7-\delta}$  compound is metallic and superconducting for  $\delta \approx 0$ , whereas it is insulating for  $\delta \approx 1$ . The positron samples essentially the  $\text{CuO}$  chains, where the oxygen atoms are added ( $\delta \approx 1$ ) or removed ( $\delta \approx 0$ ), and this effect has been studied earlier by 2D-ACAR measurements and calculations [13, 14, 26]. The main observations are the disappearance of the ridge FS, a tetragonal 2D-ACAR picture associated with the chain region symmetry, and probably a different trapping mechanism for the  $\text{YBa}_2\text{Cu}_3\text{O}_6$  compound [27]. Concerning the relation between 2D-ACAR data and  $T_c$ , it is worth mentioning that  $T_c$  remains high for a large oxygen deficiency, whereas the 2D-ACAR picture becomes very different (see [14] and results below); the orthorhombic symmetry replaced by tetragonal symmetry (of the  $\text{O}_6$  compound) and the ridge disappears. A similar behavior is observed in Al doped samples in which the Al atoms substitute with the Cu atoms of the chains,  $T_c$  decreases slowly with Al concentration, in contrast with Zn or

Ni doped samples, where the dopants substitute the Cu atoms of the plane. This is confirmed by 2D-ACAR pictures [14] which remain unchanged for Ni and Zn substitutions, whereas for Al the picture is largely disturbed, the 2D-ACAR shows tetragonal symmetry and the ridge FS vanishes.

Here we present the evolution of the 2D-ACAR in  $\text{YBa}_2\text{Cu}_3\text{O}_{7-\delta}$  for intermediate  $\delta$  values, using the same  $3 \times 2.3 \times 0.1 \text{ mm}^3$  twinned sample submitted to different heat treatments. First, the crystal was measured as grown (using the flux technique [23]). Then the sample was heated for 7 days at  $450^\circ\text{C}$  in 1 atm. of oxygen. Finally the sample was heated during 3 days at  $T = 684^\circ\text{C}$  in 1 atm. of oxygen and quenched [28]. The characterization of the sample is summarized in Table. The oxygen deficiency  $\delta$  was estimated in two ways: firstly by measuring

TABLE

Characterizations of the oxygen deficient  $\text{YBa}_2\text{Cu}_3\text{O}_{7-\delta}$  sample. The value in brackets is unreliable. See text for more details.

Sample treatment	As-grown	$684^\circ\text{C}$	$450^\circ\text{C}$
$T_c$	$(68 \pm 5 \text{ K})$	$50.5 \pm 0.5 \text{ K}$	$90.5 \pm 0.5 \text{ K}$
$c$	$11.765 \pm 0.001 \text{ \AA}$	$11.742 \pm 0.001 \text{ \AA}$	$11.705 \pm 0.001 \text{ \AA}$
$\delta$	$> 0.6$	$\approx 0.4$	$< 0.1$

$T_c$  by AC susceptibility measurements ( $\chi_{AC}$ ), and secondly the lattice parameter  $c$  was measured by X-ray diffractometry (XRD) and related to  $\delta$  using a graph shown in Ref. [29] (and references therein). This determination is possible after rescaling the  $c$ -parameter axis, since a shift may appear easily due to the large sensitivity of the  $c$ -parameter to the sample preparation. One must be careful with such estimations of  $\delta$  [30], for example, at room temperature, an exponential-like decrease of the  $c$ -parameter with time has been observed [31]. Both XRD and  $\chi_{AC}$  indicate similar  $\delta$  values in two cases ( $\delta < 0.1$  and  $\delta \approx 0.4$ ). In the third case there is a conflict. This is not surprising since the transition width ( $\pm 5 \text{ K}$ ) suggests an important oxygen inhomogeneity in the sample. In this case,  $\chi_{AC}$  leads to a small  $\delta$  value ( $< 0.4$ ), but the value implied by positron annihilation (see below) sides with the XRD value, that is  $\delta > 0.6$ . Positrons probe the whole sample volume and therefore give better bulk characterizations than surface measurements such as X-rays, or the  $\chi_{AC}$  technique which can be affected by local inhomogeneity.

Figure 5 shows the filtered  $c$ -integrated 2D-ACAR of  $\text{YBa}_2\text{Cu}_3\text{O}_{7-\delta}$ , for the three oxygen contents  $\delta$ . These pictures differ slightly from the other filtered data shown in this paper because this sample is twinned. For the  $c$  integration, the twinning acts as a superposition of two spectra different by 90 degree rotation around the  $c$ -axis. In the  $\delta \approx 0$  measurement (Fig. 5a) the ridge FS, labelled  $R$ , is clearly seen with a half width of about  $\approx 0.5 \text{ mrad}$ . This structure decreases in intensity for  $\delta \approx 0.4$  (Fig. 5b), without any significant change in width, and disappears for larger  $\delta$  (Fig. 5c). We have also observed such trends previously by analyzing the anisotropic part of the 2D-ACAR [15] and looking at the 2nd ridge FS Umklapp component. In Figs. 5a and 5b, the decrease in the FS signal,

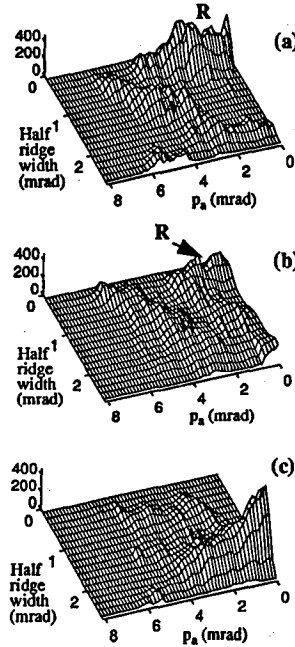


Fig. 5. Filtered normalized 2D-ACAR of twinned  $\text{YBa}_2\text{Cu}_3\text{O}_{7-\delta}$  integrated along the  $c$ -axis, measured for three oxygen contents  $\delta < 0.1$  (a),  $\delta \approx 0.4$  (b) and  $\delta > 0.6$  (c). Coordinates of the basal plane: momentum  $p_a$ , and the half width of the ridge-like structures. Vertical scale: arbitrary. Only the positive amplitudes are shown.  $R$  is for ridge,  $W$  for wave function.

averaged over the 1st BZ ( $|p_a| < 3.15$  mrad), is  $0.5 \pm 0.05$  from the  $\delta \approx 0.1$  case to the  $\delta \approx 0.4$  case. The similarity in the ridge FS width is consistent with photoemission measurements [32], where the barrel FS sizes are similar for  $\delta \approx 0.1$  and for  $\delta \approx 0.65$ . Beside the ridge, in all three figures, a 2 mrad wide structure  $W$  is seen, which becomes stronger as  $\delta$  increases. The origin of this structure is wave function effects. Thus removing oxygen atoms from the  $\text{CuO}$  chains hollows out the 2D-ACAR 2 mrad onwards along the  $a/b$  axes. This gives rise to a hump in the anisotropic part of the measured and calculated 2D-ACAR along the (110) diagonal already observed earlier [14, 18], and restores the tetragonal symmetry.

LDA calculations do not exist for comparison, since partially oxygenated  $\text{YBa}_2\text{Cu}_3\text{O}_{7-\delta}$  samples are disordered systems. Local ordering may occur, but not globally. However, for well annealed oxygen deficient samples, a dominant ordered form appears over a large range of oxygen concentration [33]: the Ortho II structure, where oxygen empty and oxygen filled chains alternate. Massidda et al. [34] performed FLAPW calculations in the ordered  $\text{YBa}_2\text{Cu}_3\text{O}_{6.5}$  compound, using a superlattice obtained by alternating, along the  $a$ -axis, the unit cells of the  $\text{O}_6$  and  $\text{O}_7$  compounds. The resulting ridge FS does not change significantly in width, but the signal is half as intense, explained by the positrons which sample roughly

equally the full and empty chains. This predicted decrease in the FS signal by 0.5 from  $\delta = 0.0$  to  $\delta = 0.5$  was expected to be slightly more important than the experimental signal ratio of 0.5 mentioned above, since in the experiment  $\delta$  varies only from 0.1 to 0.4. However, for  $\delta = 0.5$  it is unlikely that the entire crystal is ordered according to the Ortho II phase as it was considered by the FLAPW calculations; the presence of insulating phase is not excluded in real crystals, and may be at the origin of the slight difference in the FS signal decrease for the experiment and the FLAPW calculations.

The observed diminution of the FS signal also agrees with the phase separation model of Mesot et al. [35]. Using neutron spectroscopy, they observe in  $\text{ErBa}_2\text{Cu}_3\text{O}_{7-\delta}$  the coexistence of three different phases present in the same sample. The proportions of the phases vary continuously with the oxygen content  $\delta$ . For  $\delta = 0.4$ , the sum of the proportions of the two phases (labelled  $A_1$  and  $A_2$  by them) able to produce a ridge FS signal gives 0.5 (taking into account the weighting of 1/2 for  $A_2$  according to the half intense FS signal predicted for this phase by FLAPW), which is the value we also found. According to this phase separation model, for  $\delta = 0.5$ , the proportion of a third phase (the  $\text{O}_6$  phase labelled  $A_3$  by them) becomes important (30%), and the extrapolated FS signal decrease would be close to 0.4. This explains the slightly overestimated value of 0.5 calculated by FLAPW as discussed in the previous paragraph. For  $\delta = 0.6$ , a reduction of 0.3 can be estimated for the FS signal from the phase separation model, however in Fig. 5c no FS is remaining. Two reasons explain the missing FS in our case: First, the sample is not homogeneously oxygenated as discussed above, and the average  $\delta$  value may be greater than 0.6 as suggested by Fig. 5c. Secondly, for small  $p_a$ , the filtered data show an intense and wide structure  $W$  induced by wave functions. The iterative way in which the filter is used has the tendency to mask the presence of smaller features in comparison with other intense structures, causing the expected small FS signal to disappear.

## 5. Conclusions

We showed that, in 2D-ACAR data measured at  $T = 300$  K, the ridge FS of  $\text{YBa}_2\text{Cu}_3\text{O}_{7-\delta}$  produces a small signal but, after applying a linear filtering technique, a clear picture of the ridge FS could be established. Its width is constant and compares well with LDA calculations, however the predicted intensities are overestimated. Calculations with reduced FS breaks increase the agreement with the experiment.

For the first time the angular variation of the 2D-ACAR projections was measured in an untwinned  $\text{DyBa}_2\text{Cu}_3\text{O}_{7-\delta}$  sample in the  $ac$  and  $bc$  planes. The ridge FS signals extracted from the filtered data are in good agreement with LMTO calculations performed in  $\text{YBa}_2\text{Cu}_3\text{O}_7$ . A 3D model of the momentum density of the ridge could be sketched out from the measured projections and compared well with LMTO calculations, despite slightly sharper momentum density features observed experimentally.

The other new topic is the oxygen dependent 2D-ACAR measurements in  $\text{YBa}_2\text{Cu}_3\text{O}_{7-\delta}$ , which showed that the deficiency  $\delta$  influences the ridge FS in intensity but not in width. This agrees with FLAPW calculations performed in

$\text{YBa}_2\text{Cu}_3\text{O}_{6.5}$ , and is also consistent with the presence of a phase separation within the sample.

It is now clear that the description in shape and size of the ridge FS of  $\text{YBa}_2\text{Cu}_3\text{O}_{7-\delta}$ , given by the band structure calculations, is confirmed by the experiment, even for partial oxygenation. Disagreements between amplitudes of measured and calculated FS may be due either to sample quality or to defects unaccounted for in theoretical concepts. Thus calculations going beyond LDA may give better results.

### Acknowledgments

We are grateful to prof. K. Yvon for putting the X-ray diffractometer to our disposal. We thank S. Massidda for the initiations to the FLAPW calculations, and W.N. Hardy for supplying us with the high quality Y-based sample. We thank M. Weger and M. Däumling for interesting discussions. This work has been supported by the Swiss National Science Foundation.

### References

- [1] *Positron Annihilation*, Eds. Zs. Kajcsos, Cs. Szecles, *Mater. Sci. Forum* **105–110**, (1992); *J. Phys. Chem. Solids* **54**, (1993).
- [2] S. Berko, in: *Momentum Distributions*, Eds. R.N. Silver, P.E. Sokol, Plenum Pub. Corp., New York 1989, p. 273; M. Peter, *IBM J. Res. Develop.* **33/3**, 333 (1989).
- [3] S. Massidda, J. Yu, A.J. Freeman, D.D. Koelling, *Phys. Rev. Lett. A* **122**, 198 (1987).
- [4] D. Singh, W.E. Pickett, E.C. von Stetten, S. Berko, *Phys. Rev. B* **42**, 2696 (1990).
- [5] A. Bansil, P.E. Mijnarends, L.C. Smedskjaer, *Phys. Rev. B* **43**, 3667 (1991).
- [6] S. Massidda, *Physica C* **169**, 137 (1990).
- [7] T. Jarlborg, B. Barbiellini, E. Boronski, P. Genoud, M. Peter, *J. Phys. Chem. Solids* **52**, 1515 (1991).
- [8] H. Haghghi, J.H. Kaiser, S. Rayner, R.N. West, J.Z. Liu, R. Shelton, R.H. Howell, F. Solar, P.A. Sterne, M.J. Fluss, *J. Phys. Chem. Solids* **52**, 1535 (1991) and *Phys. Rev. Lett.* **67**, 38 (1991).
- [9] L.C. Smedskjaer, A. Bansil, U. Welp, Y. Fang, K.G. Bailey, *Physica C* **192**, 259 (1992).
- [10] A. Shukla, L. Hoffmann, A.A. Manuel, E. Walker, B. Barbiellini, M. Peter, *Phys. Rev. B*, to be published.
- [11] L.C. Smedskjaer, A. Bansil, U. Welp, Y. Fang, K.G. Bailay, *J. Phys. Chem. Solids* **52**, 1541 (1991).
- [12] Gh. Adam, S. Adam, B. Barbiellini, L. Hoffmann, A.A. Manuel, S. Massidda, M. Peter, *Solid State Comm.* **88**, 739 (1993).
- [13] M. Peter, A.A. Manuel, L. Hoffmann, W. Sadowski, *Europhys. Lett.* **18**, 313 (1992).
- [14] A.A. Manuel, B. Barbiellini, M. Gauthier, L. Hoffmann, T. Jarlborg, S. Massidda, M. Peter, W. Sadowski, A. Shukla, E. Walker, *J. Phys. Chem. Solids* **54**, 1223 (1993).

- [15] L. Hoffmann, A.A. Manuel, M. Peter, E. Walker, M. Gauthier, A. Shukla, B. Barbiellini, S. Massidda, Gh. Adam, S. Adam, W.N. Hardy, Ruixing Liang, *Phys. Rev. Lett.* **71**, 4047 (1993).
- [16] L. Hoffmann, A. Shukla, M. Peter, B. Barbiellini, A.A. Manuel, *Nucl. Instrum. Methods Phys. Res. A* **335**, 276 (1993).
- [17] R.N. West, in: *Positron Spectroscopy of Solids*, Eds. A. Dupasquier, A.P. Mills Jr., North-Holland, 1995, to be published.
- [18] B. Barbiellini, P. Genoud, J.Y. Henry, L. Hoffmann, T. Jarlborg, A.A. Manuel, S. Massidda, M. Peter, W. Sadowski, H.J. Scheel, A. Shukla, A.K. Singh, E. Walker, *Phys. Rev. B* **43**, 7810 (1991).
- [19] P. Genoud, Ph. D. Thesis, Geneva University, 1990.
- [20] B. Barbiellini, P. Genoud, T. Jarlborg, *J. Phys. Condens. Matter* **3**, 7631 (1991), B. Barbiellini, P. Genoud, P. Lerch, T. Jarlborg, M. Peter, in: *Positron Annihilation*, Eds. Zs. Kajcsos, Cs. Szeles, *Mater. Sci. Forum* **105**, 559 (1992).
- [21] B. Barbiellini, T. Jarlborg, M. Gauthier, A. Shukla, *Helv. Phys. Acta* **65**, 840 (1992).
- [22] M. Weger, private communication, M. Weger, *J. Low Temp. Physics* **95**, 131 (1994).
- [23] W. Sadowski, E. Walker, G. Triscone, *Physica C* **157**, 897 (1989).
- [24] H. Schmid, E. Burkhardt, B.N. Sun, J.P. Rivera, *Physica C* **157**, 555 (1989).
- [25] L.C. Smedskjaer, A. Bansil, U. Welp, Y. Fang, K.G. Bailey, *Phys. Rev. B* **46**, 5868 (1992).
- [26] B. Barbiellini, M. Gauthier, L. Hoffmann, T. Jarlborg, A.A. Manuel, S. Massidda, M. Peter, W. Sadowski, A. Shukla, E. Walker, *Physica C* **209**, 75 (1993).
- [27] L.C. Smedskjaer, A. Bansil, *J. Phys. Chem. Solids* **53**, 1657 (1992).
- [28] T. Graf, G. Triscone, J. Muller, *J. Less-Common Met.* **159**, 349 (1990).
- [29] R.J. Cava, A.W. Hewat, E.A. Hewat, B. Batlogg, M. Marezio, K.M. Rabe, J.J. Krajewski, W.F. Peck Jr., L.W. Rupp Jr., *Physica C* **165**, 419 (1990).
- [30] M. Däumling, private communication.
- [31] J.D. Jorgensen, S. Pei, P. Lightfoot, H. Shi, A.P. Paulikas, B.W. Veal, *Physica C* **167**, 571 (1990).
- [32] R. Liu, B.W. Veal, A.P. Paulikas, J.W. Downey, H. Shi, C.G. Olson, C. Gu, A.J. Arko, J.J. Joyce, R.J. Bartlett, *J. Phys. Chem. Solids* **52**, 1437 (1991).
- [33] D. deFontaine, G. Ceder, M. Asta, *J. Less-Common Met.* **164-165**, 108 (1990).
- [34] S. Massidda, J. Yu, A.J. Freeman., L. Hoffmann, P. Genoud, A.A. Manuel, *J. Phys. Chem. Solids* **52**, 1503 (1991).
- [35] J. Mesot, P. Allenspach, U. Staub, A. Furrer, H. Mutka, *Phys. Rev. Lett.* **70**, 865 (1993).